



OPEN

# In situ decorated pd NPs on Triazin-encapsulated $\text{Fe}_3\text{O}_4/\text{SiO}_2\text{-NH}_2$ as magnetic catalyst for the synthesis of diaryl ethers and oxidation of sulfides

Durgesh Singh<sup>1✉</sup>, Kamini Singh<sup>2</sup>, Pawan Sharma<sup>3,4</sup>, Yashwantsinh Jadeja<sup>5</sup>, Johar MGM<sup>6</sup>, Priyanka Singh<sup>7</sup>, Kiranjeet Kaur<sup>8</sup>, M. Atif<sup>9</sup>, Mohammed A. El-Meligy<sup>10,11</sup> & Beneen Hussein<sup>12,13</sup>

This article is devoted to the synthesis of a new magnetic palladium catalyst that has been immobilized on A-TT-Pd coated-magnetic  $\text{Fe}_3\text{O}_4$  nanoparticles. Such surface functionalization of magnetic particles is a promising method to bridge the gap between heterogeneous and homogeneous catalysis approaches. The structure, morphology, and physicochemical properties of the particles were characterized through different analytical techniques, including TEM, FT-IR, XRD, SEM, EDS, TGA-DTG, ICP, and VSM techniques. The obtained  $\text{Fe}_3\text{O}_4@\text{SiO}_2@\text{A-TT-Pd}$  performance can show excellent catalytic activity for the synthesis of diaryl ethers and oxidation of sulfides, and the corresponding products were obtained with high yields. The advantages of this catalyst include a simple test method, green reaction conditions, no use of dangerous solvents, short reaction time, low catalyst loading, and reusability. Also, the nanocatalyst was easily separated from the reaction mixture with the help of a bar magnet and recovered and reused several times without loss of stability and activity.

**Keywords** Complex, Sulfides, Triazin, Ether,  $\text{Fe}_3\text{O}_4$

Nanomaterials that can be magnetically separated are considered one of the most significant material classes due to their distinct physicochemical properties. They have garnered interest from a diverse group of researchers<sup>1,2</sup>. With their potential as green heterogeneous catalysts in diverse organic functional group transformations and as catalytic supports, spinel ferrite compounds show great promise for use in industry and technology<sup>3</sup>. Over the last ten years, magnetic nanoparticles have been extensively used as a support in the production of magnetic nanocatalysts due to their simple preparation and easy retrieval using a magnetic field<sup>4</sup>. The easy separation of these nanoparticles from the reaction mixture using an external magnet is one of the benefits of magnetic nanoparticles<sup>5</sup>. The field of catalysis science plays a central role in numerous crucial organic reactions. Many essential organic functional group transformations necessitate the presence of a catalyst in the reaction environment to enable the selective conversion of reagents and synthons into the desired products with high efficiency<sup>6</sup>. The use of diverse nanomaterials as catalysts has globally captivated attention because of their

<sup>1</sup>Department of Chemistry, School of Chemical Sciences and Technology, Dr. Harisingh Gour Vishwavidyalaya (A Central University), Sagar 470003, India. <sup>2</sup>Department of Chemistry, Deen Dayal Upadhyay Gorakhpur University, Gorakhpur 273009, India. <sup>3</sup>Department of Chemistry, School of Sciences, Jain (Deemed-to-be) University, Bengaluru 560069, Karnataka, India. <sup>4</sup>Department of Sciences, Vivekananda Global University, Jaipur, Rajasthan 303012, India. <sup>5</sup>Marwadi University Research Center, Department of Chemistry, Faculty of Science, Marwadi University, Rajkot 360003, Gujarat, India. <sup>6</sup>Management and Science University, Shah Alam, Selangor, Malaysia. <sup>7</sup>NIMS School of Allied Sciences and Technology, NIMS University, Rajasthan, Jaipur 303121, India. <sup>8</sup>Chandigarh Pharmacy College, Chandigarh Group of colleges-Jhanjeri, Mohali 140307, Punjab, India. <sup>9</sup>Department of Physics and Astronomy, College of Science, King Saud University, P O Box 2455, Riyadh 11451, Saudi Arabia. <sup>10</sup>Jadara University Research Center, Jadara University, P O Box 733, Irbid, Jordan. <sup>11</sup>Applied Science Research Center, Applied Science Private University, Amman, Jordan. <sup>12</sup>Medical laboratory technique college, the Islamic University, Najaf, Iraq. <sup>13</sup>Medical laboratory technique college, the Islamic University of Al Diwaniyah, Al Diwaniyah, Iraq. ✉email: durgesh.phdchem16@gmail.com

distinctive ability to transform manufacturing processes into environmentally friendly, more sustainable, and cost-effective methods<sup>7</sup>. Among heterogeneous catalysts,  $\text{Fe}_3\text{O}_4$  has been greatly favored since they are simply synthesized and surface-modified using a magnet<sup>8,9</sup>. Different catalysts can be supported on  $\text{Fe}_3\text{O}_4$  nanoparticles due to easy separation after several reuses. Over the past decade, scientists have achieved a significant milestone with the discovery of the C-O coupling reaction facilitated by palladium-containing complexes<sup>10,11</sup>. Transition metal catalyst systems have greatly transformed the synthesis of organic structures through carbon-heteroatom coupling reactions<sup>12–14</sup>. These model reactions are extensively utilized in the synthesis of pharmaceutical, agricultural, and chemical compounds<sup>15–17</sup>. Diaryl ethers are ubiquitous in targeted synthetic and natural products, including agricultural and pharmaceutical chemicals, pharmaceuticals, fragrances, and flavorings<sup>18,19</sup>.

The targeted oxidation of organic sulfur compounds holds significant importance in biological, synthetic, and industrial contexts<sup>20</sup>. Sulfides play crucial roles in both biological and industrial processes<sup>21</sup>. They serve as significant reagents in organic synthesis, acting as protective agents for thiol, facilitating sulfonylation of enolates and other anions, and enabling the synthesis of organo-sulfur compounds through C-S bond formation<sup>22</sup>. Moreover, they are essential starting materials for the preparation of sulfinyl and sulfonyl reagents<sup>23</sup>. The selective oxidation of sulfides to sulfoxides holds great significance in organic chemistry<sup>24</sup>. Some biologically active sulfoxides are crucial as therapeutic agents, serving as antifungal, antibacterial, anti-atherosclerotic, anti-ulcer, antihypertensive, psychotropic, and vasodilator compounds<sup>25</sup>. A variety of methods, such as different catalysts and various oxidants, have been employed for the selective oxidation of organic sulfides and thiols. In this context, the use of  $\text{H}_2\text{O}_2$  as a green oxidant has garnered significant interest due to its environmental implications, accessibility, high atom efficiency, and relatively lower costs compared to other oxidizing agents<sup>26</sup>.

Considering the interesting benefits of heterogeneous catalysts with the use of novel and green materials, herein, we reported the synthesis of an efficient and heterogeneous novel A-TT-Pd coated on  $\text{Fe}_3\text{O}_4$  MNPs and its application in the synthesis of diaryl ethers and oxidation of sulfides in high yields under mild conditions.

## Experimental

### Preparation of $\text{Fe}_3\text{O}_4@\text{SiO}_2@\text{A-TT-Pd}$

For the synthesis of  $\text{Fe}_3\text{O}_4$  nanoparticles, a mixture of  $\text{FeCl}_2 \cdot 3\text{H}_2\text{O}$  (2 g) and  $\text{FeCl}_3 \cdot 6\text{H}_2\text{O}$  (4 g) in 25 mL ethanol at room temperature was added to a round bottom flask. After adding 2 g of NaOH to the reaction container, the solution was vigorously stirred at 80 °C for 48 h. Subsequently, the prepared magnetic nanoparticles were separated using a magnet, washed with deionized water, and dried at 60 °C for 10 h. Following this, 1 gram of the obtained  $\text{Fe}_3\text{O}_4$  was dispersed in a mixture of 40 mL of ethanol, 5.0 mL of ammonia solution, and 20 mL of  $\text{H}_2\text{O}$ . Then, 2 g of PEG-400 and 3 mL of tetraethyl orthosilicate (TEOS) were added to the mixture, which was stirred for 24 h at room temperature. The resulting product ( $\text{Fe}_3\text{O}_4@\text{SiO}_2$ ) was then separated using an external magnet, subjected to multiple washes with ethanol and  $\text{H}_2\text{O}$ , and dried at 25 °C (Scheme 1)<sup>27,28</sup>. To synthesize the  $\text{Fe}_3\text{O}_4@\text{SiO}_2@\text{A}$  complex, 1 g of the prepared  $\text{Fe}_3\text{O}_4@\text{SiO}_2$  was dispersed in 30 mL EtOH by sonication for 30 min. After that, 3 mmol of 3-aminopropyltriethoxysilane (A) was introduced into the reaction container and stirred under reflux conditions for 24 h. Following the completion of the reaction, the  $\text{Fe}_3\text{O}_4@\text{SiO}_2@\text{A}$  product was isolated using a magnet and subsequently cleansed with ethyl acetate and EtOH, before being dried at 50 °C in an oven for 15 h. The initial step in the preparation of  $\text{Fe}_3\text{O}_4@\text{SiO}_2@\text{A@T}$  involved dispersing 1 g of  $\text{Fe}_3\text{O}_4@\text{SiO}_2@\text{A}$  samples in 20 mL of toluene. Subsequently, 2.5 mmol of trimethylamine ( $\text{Et}_3\text{N}$ ) and 2.5 mmol of 1,3,5-trichloro triazine were added as a cross-linking reagent to the reaction mixture, which was then refluxed for 24 h. The  $\text{Fe}_3\text{O}_4@\text{SiO}_2@\text{A@T}$  were subsequently separated with the help of an external magnet, cleaned with EtOH, and dried. In the continuation of the nanocatalyst synthesis,  $\text{Fe}_3\text{O}_4@\text{SiO}_2@\text{A@T}$  (1 g) was reacted with tris(hydroxymethyl)amino methane (0.6 g) and  $\text{Et}_3\text{N}$  (1.5 mmol) in dry toluene. The mixture was stirred for 24 h at a temperature of 70 °C. Following this duration, the separation, washing, and drying process was carried out as the final step. Finally, to prepare  $\text{Fe}_3\text{O}_4@\text{SiO}_2@\text{A@TT-Pd}$  organometallic catalytic, a mixture of  $\text{Fe}_3\text{O}_4@\text{SiO}_2@\text{A@TT}$  (1.0 g), Palladium (II) acetate (2.5 mmol) and 50 ml ethanol was added into the flask, and it was stirred at reflux condition for 24 h. Also, 2 mmol of  $\text{NaBH}_4$  was added to the reaction mixture and stirred for 4 h. After the completion of the reaction, the  $\text{Fe}_3\text{O}_4@\text{SiO}_2@\text{A-TT-Pd}$  catalyst was separated and washed with  $\text{H}_2\text{O}$  and ethanol and dried in vacuum.

### Aromatic ethers formation catalyzed by $\text{Fe}_3\text{O}_4@\text{SiO}_2@\text{A-TT-Pd}$

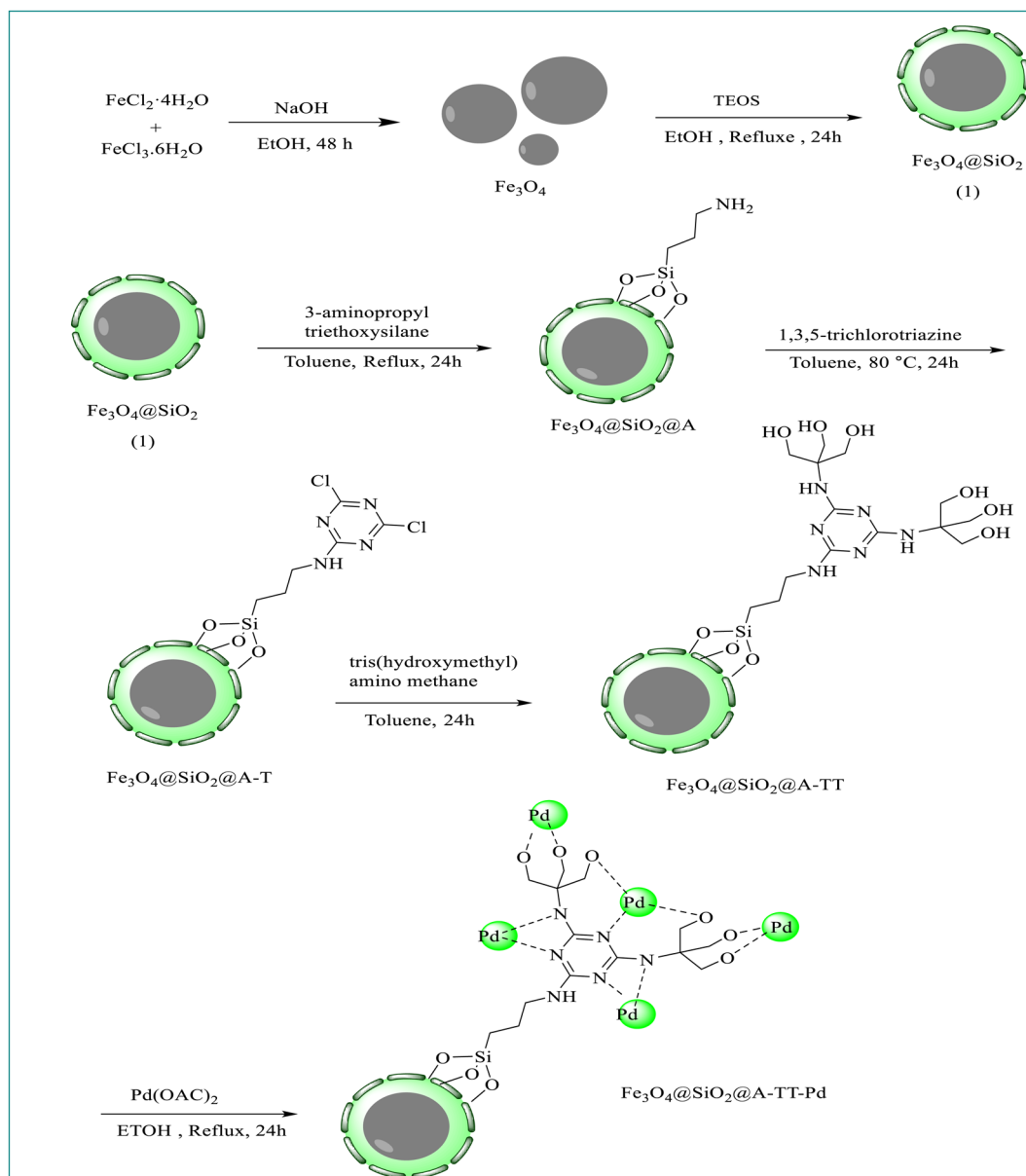
Aryl halide (1 mmol), KOH (5 mmol), phenol (1 mmol), and  $\text{Fe}_3\text{O}_4@\text{SiO}_2@\text{A-TT-Pd}$  (30 mg) were stirred in  $\text{H}_2\text{O}$  at 70 °C and the progression of the reaction was seen by TLC. After completing the reaction, the reaction mixture was cooled to room temperature. Subsequently, water was added to dilute the mixture, and the residual catalyst was removed using an external magnet and then rinsed with ethyl acetate. The resulting solution was filtered and then separated into ethyl acetate and water layers. The  $\text{Na}_2\text{SO}_4$  (2 g) was used to dry the solution, after which the solvent was evaporated, yielding pure ether derivatives (Scheme 2).

### A general procedure for the oxidation of sulfides

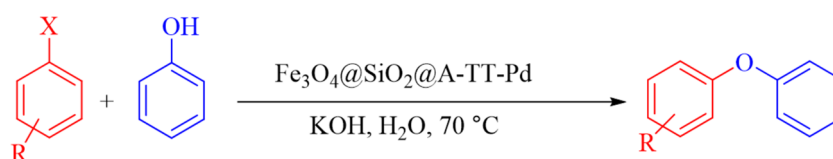
A combination of sulfide (2 mmol) and  $\text{H}_2\text{O}_2$  33% (0.3 mL) was poured into the round-bottomed flask containing  $\text{Fe}_3\text{O}_4@\text{SiO}_2@\text{A-TT-Pd}$  (0.02 g). The mixture was stirred at room temperature, and the progress of the reaction was monitored by TLC. At the end of the reaction, the catalyst was removed by a magnet, and the products were extracted by water and ethyl acetate. The organic solvents were dried over anhydrous  $\text{Na}_2\text{SO}_4$ . Then, the organic solvent was evaporated, and pure products were obtained in high yields (Scheme 3).

### Selected NMR data

Oxydibenzene:  $^1\text{H}$  NMR (400 MHz, DMSO):  $\delta_{\text{H}} = 7.04$  (m, 5 H), 6.83 (m, 5 H) ppm.



**Scheme 1.** Schematic diagram of Fe<sub>3</sub>O<sub>4</sub>@SiO<sub>2</sub>@A-TT-Pd.



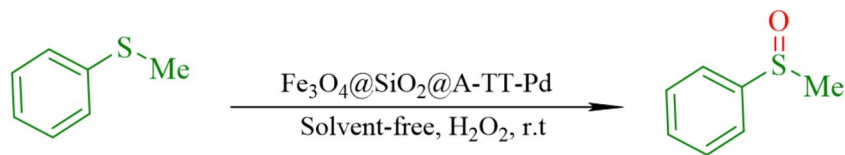
**Scheme 2.** Synthesis of diaryl ether derivatives using Fe<sub>3</sub>O<sub>4</sub>@SiO<sub>2</sub>@A-TT-Pd.

1-Methoxy-4-phenoxybenzene: <sup>1</sup>H NMR (400 MHz, DMSO): δ<sub>H</sub> = 7.47 (d, 1 H), 7.34 (d, 5 H), 7.18 (s, 3 H), 7.18 (s, 3 H) ppm.

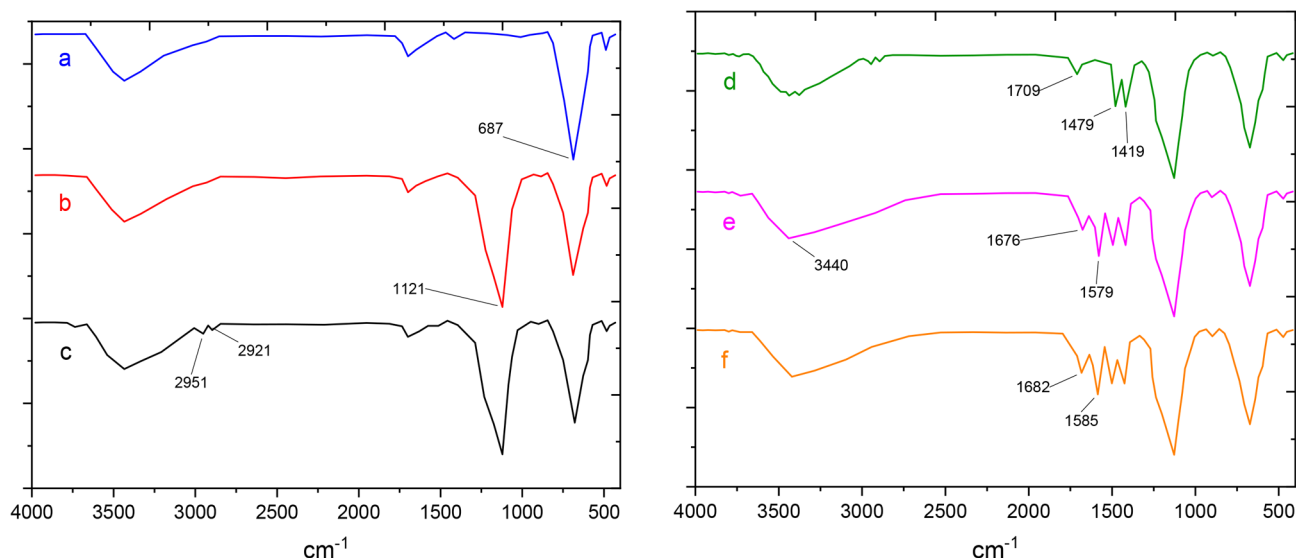
1-Nitro-4-phenoxybenzene: <sup>1</sup>H NMR (MHz, DMSO): δ<sub>H</sub> = 7.95 (d, 3 H), 7.39 (d, 4 H), 7.07 (s, 2 H) ppm  
 (Sulfinylbis(methylene))dibenzene: <sup>1</sup>H NMR (400 MHz, DMSO): δ<sub>H</sub> = 7.56 (d, 5 H), 7.28 (d, 5 H), 4.07 (s, 4 H) ppm.

(Ethylsulfinyl)ethane: <sup>1</sup>H NMR (400 MHz, DMSO): δ<sub>H</sub> = 2.71 (m, 4 H), 1.14 (d, 6 H) ppm.

(Benzylsulfinyl)benzene: <sup>1</sup>H NMR (400 MHz, DMSO): δ<sub>H</sub> = 2.34 (m, 10 H), 4.17 (d, 2 H) ppm.



**Scheme 3.** Oxidation of sulfides catalyzed by  $\text{Fe}_3\text{O}_4@\text{SiO}_2@\text{A-TT-Pd}$ .



**Fig. 1.** Comparative study of FT-IR spectra of (a)  $\text{Fe}_3\text{O}_4$ , (b)  $\text{Fe}_3\text{O}_4@\text{SiO}_2$ , (c)  $\text{Fe}_3\text{O}_4@\text{SiO}_2@\text{A}$ ,  $\text{Fe}_3\text{O}_4@\text{SiO}_2@\text{A@T}$ , (d)  $\text{Fe}_3\text{O}_4@\text{SiO}_2@\text{A@TT}$ , (e)  $\text{Fe}_3\text{O}_4@\text{SiO}_2@\text{A-TT-Pd}$ .

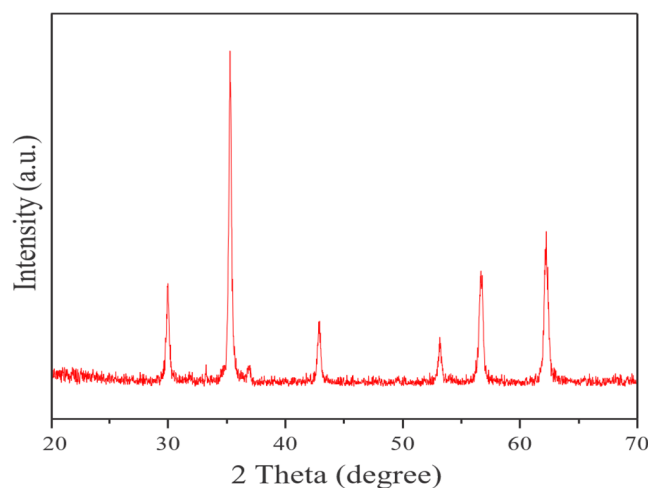
#### Catalyst characterizations

The FTIR spectra of  $\text{Fe}_3\text{O}_4$ ,  $\text{Fe}_3\text{O}_4@\text{SiO}_2$ ,  $\text{Fe}_3\text{O}_4@\text{SiO}_2@\text{A}$ ,  $\text{Fe}_3\text{O}_4@\text{SiO}_2@\text{A@T}$ ,  $\text{Fe}_3\text{O}_4@\text{SiO}_2@\text{A@TT}$ , and  $\text{Fe}_3\text{O}_4@\text{SiO}_2@\text{A-TT-Pd}$  are shown in Fig. 1. A sharp peak at  $678\text{ cm}^{-1}$  in the FT-IR spectrum of bare  $\text{Fe}_3\text{O}_4$  is related to the Fe–O vibrations (Fig. 1a). After encapsulation of  $\text{Fe}_3\text{O}_4$  MNPs, one new peak appears at  $1121\text{ cm}^{-1}$  in the FTIR spectrum, which is related to the stretching vibration of Si–O–Si, which is not indicated in the FTIR spectrum of bare  $\text{Fe}_3\text{O}_4$ . Furthermore, the stretching vibration of the surface O–H appeared as a broad peak above  $3400\text{ cm}^{-1}$  in the FT-IR spectra (Fig. 1b). The surface modification of  $\text{Fe}_3\text{O}_4@\text{SiO}_2$  by APTMS was confirmed by the emergence of multiple new peaks at  $>3000\text{ cm}^{-1}$ , corresponding to the vibration of aliphatic  $\text{CH}_2$  groups in the propyl chain. This characteristic was not observed in the FT-IR spectrum of  $\text{Fe}_3\text{O}_4@\text{SiO}_2$  (Fig. 1c). After modifying the nanoparticles with cyanuric chloride, three bands at  $1709$ ,  $1479$ , and  $1419\text{ cm}^{-1}$  appeared, possibly corresponding to the aromatic ring of cyanuric chloride (Fig. 1d). Following the immobilization of tris(hydroxymethyl)amino methane on nanoparticles, a distinctive peak emerges at  $1579\text{ cm}^{-1}$ , potentially indicative of the bending vibration of N–H groups. Also, the peak appearing in the region of  $2500\text{--}3400$  is related to the hydroxy ligand group of tris(hydroxymethyl)amino methane (Fig. 1e). More importantly, the change in the intensity of the peaks of  $\text{Fe}_3\text{O}_4@\text{SiO}_2@\text{A@TT-Pd}$  confirms the coordination of the nitrogen atom of the amino groups to Pd (Fig. 1f).

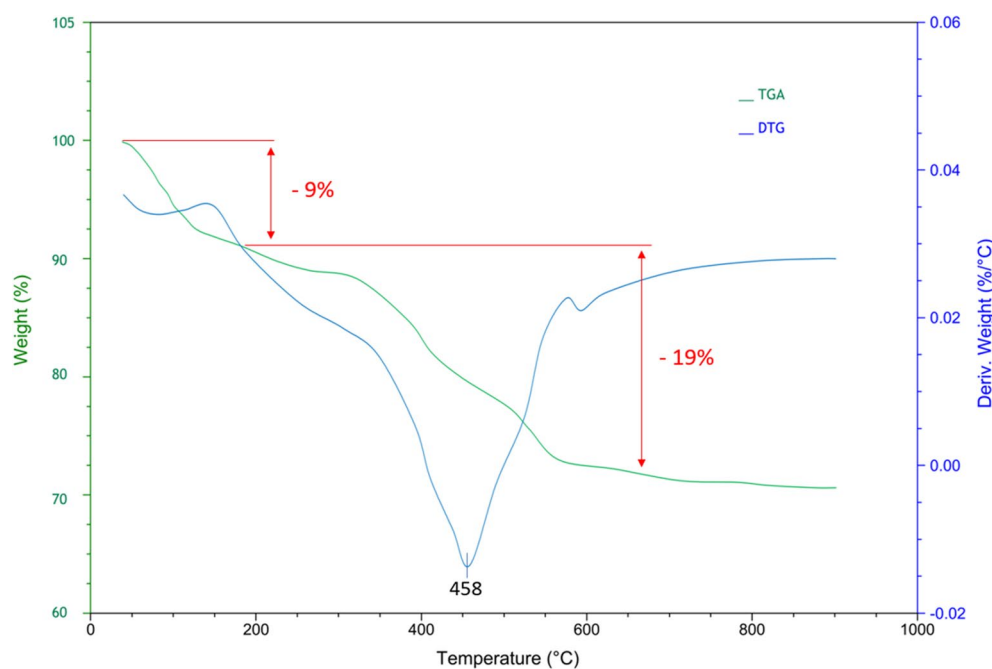
The diffraction patterns of  $\text{Fe}_3\text{O}_4@\text{SiO}_2@\text{A-TT-Pd}$  are depicted in Fig. 2. A study using powder X-ray diffraction (XRD) was conducted to analyze the phase behavior and crystallinity of the catalyst. The initial phases in the  $2\theta$  region up to  $30^\circ$ ,  $36^\circ$ ,  $45^\circ$ ,  $54^\circ$ ,  $57^\circ$ , and  $64^\circ$  were identified as the (2 2 0), (3 1 1), (4 0 0), (4 2 2), (5 1 1), and (4 4 0) planes of the highly crystalline  $\text{Fe}_3\text{O}_4@\text{SiO}_2@\text{A-TT-Pd}$  nanostructure. The XRD pattern of the catalyst indicates that the  $\text{Fe}_3\text{O}_4$  phase remained unchanged following the modifications with a distinct organic functional group (Fig. 2).

The TGA-DTG curve of  $\text{Fe}_3\text{O}_4@\text{SiO}_2@\text{A-TT-Pd}$  indicated a weight loss of 9% below  $200^\circ\text{C}$  which corresponds to desorption of physically adsorbed solvents. The most significant weight loss, about 19%, occurs within the temperature range of  $200$  to  $600^\circ\text{C}$ , and it is associated with the elimination of organic compounds from  $\text{Fe}_3\text{O}_4$  (see Fig. 3), which shows the thermal stability of the mentioned catalyst up to a temperature of  $600^\circ\text{C}$ . Also, the successful attachment of A-TT-Pd to the surface of  $\text{Fe}_3\text{O}_4$  MNPs was confirmed through the results of TGA analysis.

EDX is one of the best approaches to determining elements present in nanoparticles and the purity of nanoparticles (Fig. 4). Figure 4 illustrates the EDX spectrum of  $\text{Fe}_3\text{O}_4@\text{SiO}_2@\text{A-TT-Pd}$  MNPs, confirming the presence of C, N, Fe, O, Si, and Pd in the catalyst and providing evidence for the successful synthesis of nanoparticles.



**Fig. 2.** XRD spectrum of  $\text{Fe}_3\text{O}_4@\text{SiO}_2@\text{A-TT-Pd}$ .



**Fig. 3.** TGA-DTG curve of  $\text{Fe}_3\text{O}_4@\text{SiO}_2@\text{A-TT-Pd}$ .

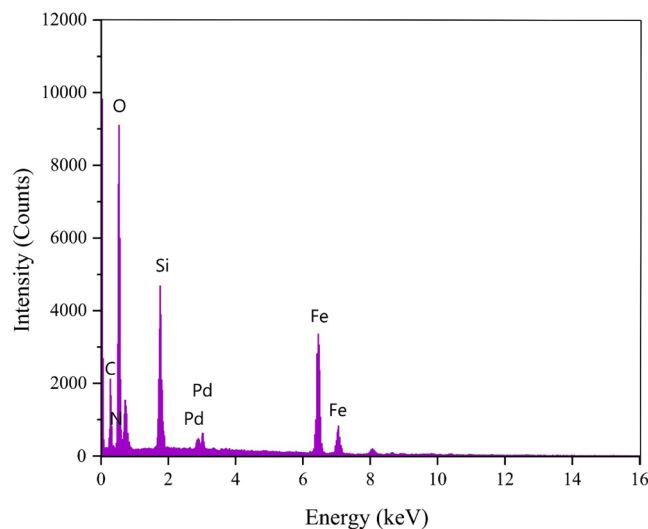
The SEM analysis revealed the morphology and dimensions of  $\text{Fe}_3\text{O}_4@\text{SiO}_2@\text{A-TT-Pd}$ . The resulting SEM image illustrated that the nanoparticles were spherical and within the nano-size range (Fig. 5).

To demonstrate the particle size distribution of these catalysts, Fig. 6 displays the histogram of particle sizes extracted from SEM images. As shown, the particle size of  $\text{Fe}_3\text{O}_4@\text{SiO}_2@\text{A-TT-Pd}$  shows homogeneous diameters in the obtained histogram SEM images.

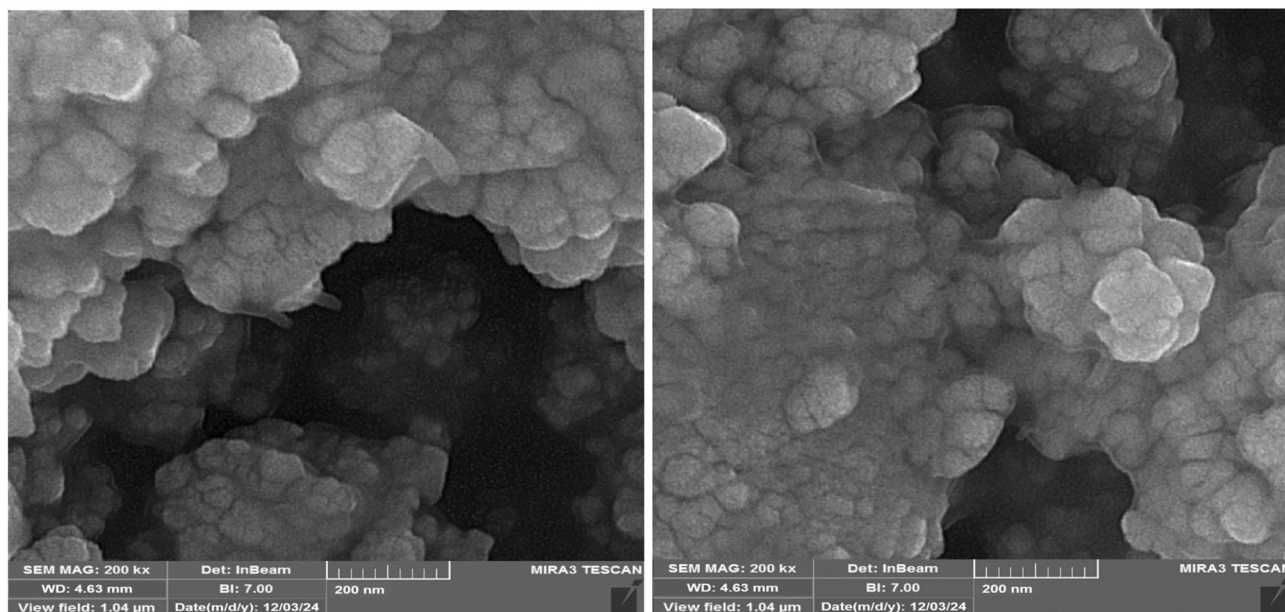
Also, the morphology of the  $\text{Fe}_3\text{O}_4@\text{SiO}_2@\text{A-TT-Pd}$  was investigated by TEM, as shown in Fig. 7. The images revealed the modified  $\text{Fe}_3\text{O}_4$  nanoparticles with TT-Pd as an organic shell covered. Images from scanning electron microscopy reveal that the catalyst particles are within the nanometer range and exhibit a spherical structure. This was further confirmed by the data obtained from transmission electron microscopy images (Fig. 7).

Furthermore, ICP-OES analysis was conducted to determine the quantity of Pd in  $\text{Fe}_3\text{O}_4@\text{SiO}_2@\text{A-TT-Pd}$ . According to the analysis, the catalyst was determined to contain  $2.4 \times 10^{-4}$  mol of Pd per gram based on ICP-OES. The Pd leaching amount after recycling the catalyst was investigated through ICP-OES analysis. Based on this analysis, the reused catalysts contain  $2.3 \times 10^{-4}$  mol.  $\text{g}^{-1}$  of Pd, indicating minimal leaching of Pd from the  $\text{Fe}_3\text{O}_4@\text{SiO}_2@\text{A-TT-Pd}$  framework.





**Fig. 4.** EDS analysis of  $\text{Fe}_3\text{O}_4@\text{SiO}_2@\text{A-TT-Pd}$ .



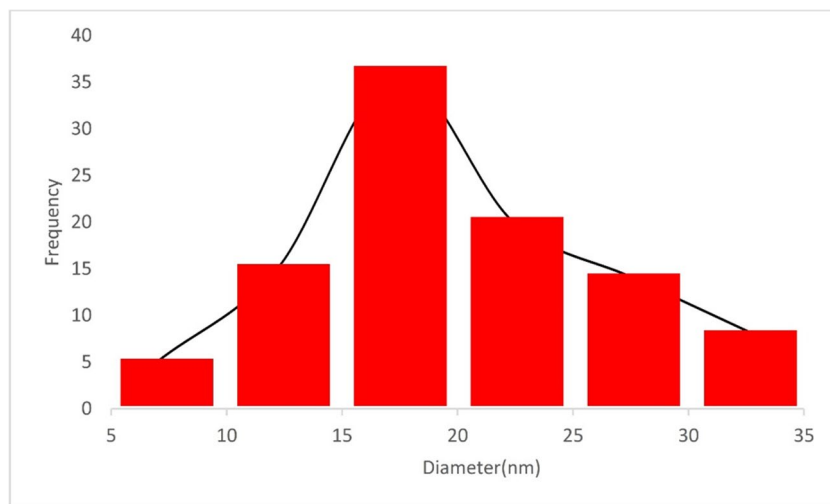
**Fig. 5.** SEM images of  $\text{Fe}_3\text{O}_4@\text{SiO}_2@\text{A-TT-Pd}$ .

The magnetic behavior of  $\text{Fe}_3\text{O}_4$  (Fig. 8a), and  $\text{Fe}_3\text{O}_4@\text{SiO}_2@\text{A-TT-Pd}$  (Fig. 8b) was investigated using VSM techniques. As expected, the decrease in saturation magnetization from about 61 emu/g to about 43 emu/g, is related to the newly coated layer (Fig. 8).

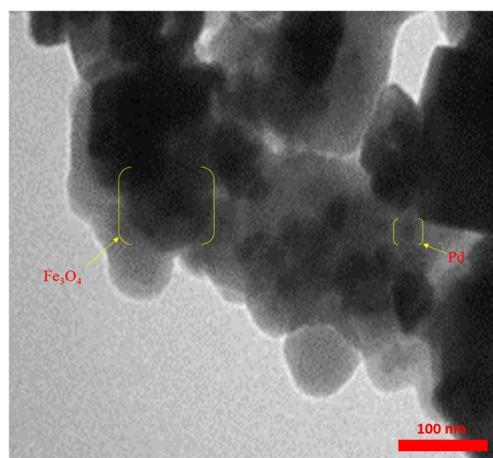
#### Catalytic studies

The catalytic activity of  $\text{Fe}_3\text{O}_4@\text{SiO}_2@\text{A-TT-Pd}$  was studied in the C-O coupling reaction for producing diaryl ether derivatives. In the production of diaryl ethers, the pairing of phenol with iodobenzene using the catalytic potential of  $\text{Fe}_3\text{O}_4@\text{SiO}_2@\text{A-TT-Pd}$  has been selected as a model reaction to determine the optimized conditions. Initially, the pattern reaction was tested without  $\text{Fe}_3\text{O}_4@\text{SiO}_2@\text{A-TT-Pd}$ , resulting in the pattern reaction not proceeding. Then, the pattern reaction was carried out using the variant value of the catalyst which was completed with 99% of yield when 0.02 g of  $\text{Fe}_3\text{O}_4@\text{SiO}_2@\text{A-TT-Pd}$  was used (Table 1). The reaction pattern was studied under a wide range of temperatures, with a focus on the effects of different solvents and bases. The best results for diaryl ether synthesis were achieved using  $\text{H}_2\text{O}$  as the solvent and KOH as the base at 70 °C, as shown in Table 1.

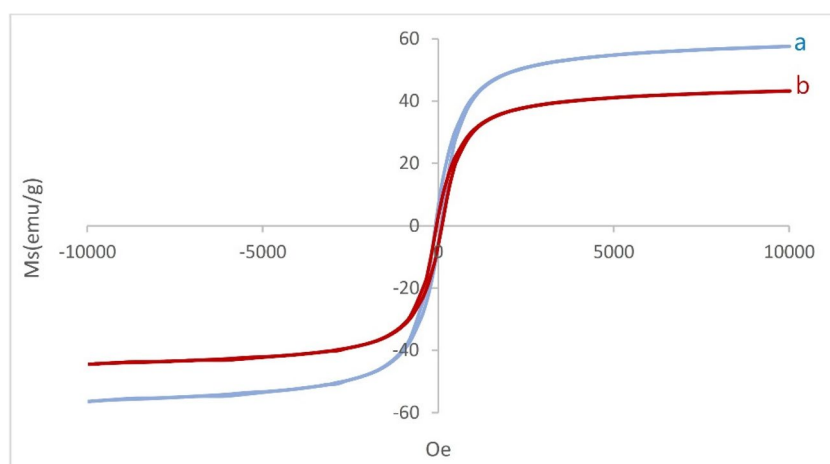
The optimizing conditions mentioned were explored for various aryl halide derivatives to broaden the catalytic scope of  $\text{Fe}_3\text{O}_4@\text{SiO}_2@\text{A-TT-Pd}$  (Table 2). Aryl halide derivatives with different functional groups,



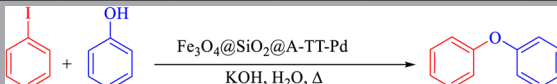
**Fig. 6.** Particle size distribution histogram of  $\text{Fe}_3\text{O}_4@\text{SiO}_2@\text{A-TT-Pd}$ .



**Fig. 7.** TEM images of  $\text{Fe}_3\text{O}_4@\text{SiO}_2@\text{A-TT-Pd}$ .



**Fig. 8.** VSM curves of (a)  $\text{Fe}_3\text{O}_4$  (b)  $\text{Fe}_3\text{O}_4@\text{SiO}_2@\text{A-TT-Pd}$ .



Entry	Catalyst (g)	Solvent	Base	Temperature (°C)	Time (min)	Yield (%) <sup>a</sup>
1	-	H <sub>2</sub> O	KOH	70	3 days	N. R
2	0.008	H <sub>2</sub> O	KOH	70	30	40
3	0.01	H <sub>2</sub> O	KOH	70	30	78
4	0.015	H <sub>2</sub> O	KOH	70	30	95
5	0.02	H <sub>2</sub> O	KOH	70	30	99
6	0.025	H <sub>2</sub> O	KOH	70	30	99
7	0.02	PEG-400	KOH	70	30	40
8	0.02	EtOAc	KOH	70	30	75
9	0.02	Acetonitrile	KOH	70	30	82
10	0.02	EtOH	KOH	70	30	89
11	0.02	H <sub>2</sub> O	Li <sub>2</sub> CO <sub>3</sub>	70	30	90
12	0.02	H <sub>2</sub> O	Na <sub>2</sub> CO <sub>3</sub>	70	30	90
13	0.02	H <sub>2</sub> O	Cs <sub>2</sub> CO <sub>3</sub>	70	30	88
14	0.02	H <sub>2</sub> O	NaHCO <sub>3</sub>	70	30	75
15	0.02	H <sub>2</sub> O	K <sub>2</sub> CO <sub>3</sub>	70	30	45
16	0.02	H <sub>2</sub> O	KOH	25	30	Trace
17	0.02	H <sub>2</sub> O	KOH	50	30	45
18	0.02	H <sub>2</sub> O	KOH	Reflux	30	99

**Table 1.** Optimization of different parameters for the reaction of phenol with iodobenzene. <sup>a</sup> Isolated yield.

whether electron-withdrawing or electron-donating in nature, were effectively coupled with phenol in high yields using this catalyst. As indicated in Table 2, aryl iodides exhibit a higher reaction rate compared to aryl bromides, while aryl chlorides demonstrate the lowest reaction rate when coupling phenol using the Fe<sub>3</sub>O<sub>4</sub>@SiO<sub>2</sub>@A-TT-Pd catalyst. This suggests that the C–Cl bond is stronger than the C–I bond, as the carbon and chlorine orbitals share similar size, energy, and symmetry, whereas the iodine and carbon orbitals differ in size and energy. Furthermore, the C–I bond is longer and weaker than the C–Cl bond, requiring less energy to break and resulting in a faster coupling rate compared to the shorter C–Cl bond. For instance, the coupling of phenol with 4-nitrobromobenzene surpasses that of 4-nitrochlorobenzene. This pattern is also evident in the coupling of phenol with iodobenzene, bromobenzene, and chlorobenzene using the Fe<sub>3</sub>O<sub>4</sub>@SiO<sub>2</sub>@A-TT-Pd catalyst.

The Carbon-Oxygen cross-coupling reaction's proposed mechanism, as depicted in Scheme 4, is based on previous findings. In the initial step, iodobenzene undergoes oxidative addition with Pd, yielding intermediate (1). Subsequently, intermediate (1) engages with phenol to generate intermediate (2), which ultimately undergoes reductive elimination to yield ether while liberating the Pd nanoparticle.

To optimize the reaction conditions, we investigated the oxidation process of methyl phenyl sulfide as a representative compound using H<sub>2</sub>O<sub>2</sub> under different reaction parameters, including time and product yield (see Table 3). As shown in Table 3, the reaction was incomplete in the absence of Fe<sub>3</sub>O<sub>4</sub>@SiO<sub>2</sub>@A-TT-Pd even after 12 h. Under solvent-free conditions at room temperature, utilizing a catalytic amount of Fe<sub>3</sub>O<sub>4</sub>@SiO<sub>2</sub>@A-TT-Pd (0.01 g), H<sub>2</sub>O<sub>2</sub> was determined to be the optimal reagent for the complete conversion of methyl phenyl sulfide to methyl phenyl sulfoxide.

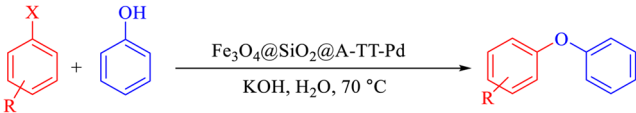
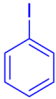
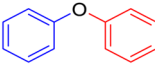

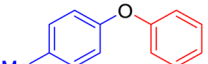

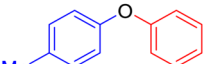
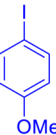
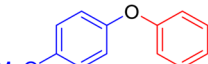
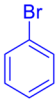
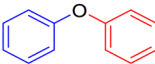

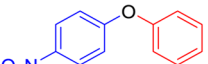

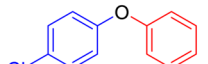

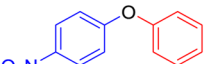
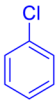
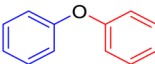

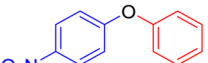
The generality of this approach has been demonstrated by facile oxidation of aryl, cyclic, benzylic, and linear as shown in Table 4. The sulfoxides were quickly obtained with high yields. To demonstrate the chemoselectivity of the protocol, sulfides containing oxidation-prone and acid-sensitive functional groups such as CHO, OH, and CO<sub>2</sub>CH<sub>3</sub> were used in the sulfoxidation reaction. Importantly, these functional groups remained unaffected during the sulfide to sulfoxide conversion, as shown in Table 4. Catalyst evaluation heavily relies on selectivity, which plays a crucial role in determining their effectiveness. Chemoselectivity specifically refers to the reactivity of a functional group when other susceptible functional groups are present and subject to the same reaction. An example of this is the oxidation of sulfide in the presence of a hydroxyl group, which can also be oxidized to form a carbonyl. The chemoselectivity of Fe<sub>3</sub>O<sub>4</sub>@SiO<sub>2</sub>@A-TT-Pd was investigated in the oxidation of 2-phenylthioethanol. This catalyst shows good chemoselectivity in synthesizing sulfoxides in the oxidation of 2-phenylthioethanol (Table 4, entry 9).

Based on previous studies, a suggested and possible mechanism for the oxidation of sulfides catalyzed by Fe<sub>3</sub>O<sub>4</sub>@SiO<sub>2</sub>@A-TT-Pd has been presented in Scheme 5. In Fe<sub>3</sub>O<sub>4</sub>@SiO<sub>2</sub>@A-TT-Pd, Palladium plays a crucial role as a magnetic nanocatalyst by forming the active oxidant complex. This mechanism facilitates the transfer of oxygen to sulfur, resulting in the formation of sulfoxide.

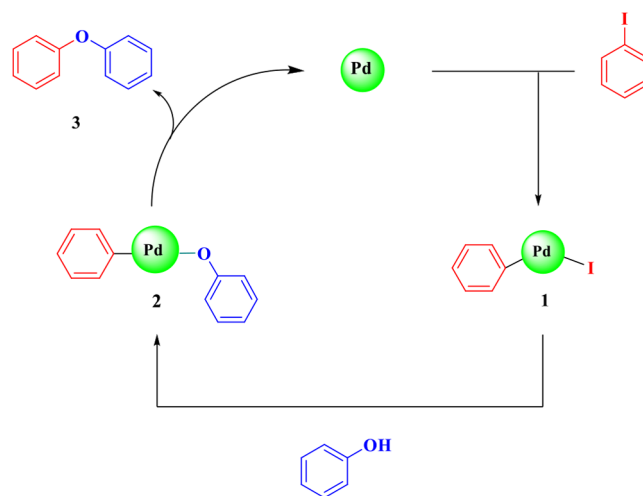
#### Hot filtration

In order to determine any leaching of palladium in the reaction mixture and to demonstrate the heterogeneous nature of Fe<sub>3</sub>O<sub>4</sub>@SiO<sub>2</sub>@A-TT-Pd catalyst, a hot filtration test was conducted during the synthesis of diaryl



						
Entry	Aryl halide	Product	Time (h)	Yield (%)	TON	TOF (min <sup>-1</sup> )
1			30 (min)	99	206	520
2			1.5	93	193.7	129.1
3			1	90	187.5	187.5
4			45 (min)	95	197.9	263.8
5			2	94	195.8	97.9
6			3.5	87	181.2	51.7
7			1.5	95	197.9	131.9
8			1.5	90	187.5	125
9			3	85	177	59
10			4.5	90	187.5	41.6

**Table 2.** Synthesis of diaryl ether derivatives using Fe<sub>3</sub>O<sub>4</sub>@SiO<sub>2</sub>@A-TT-Pd.



**Scheme 4.** Proposed mechanism for C–O cross-coupling.

Entry	Catalyst(g)	Solvent	H <sub>2</sub> O <sub>2</sub> (mg)	Time (min)	Yield
1	-	Solvent-free	0.3	12 h	Trace
2	0.005	Solvent-free	0.3	15	60
3	0.07	Solvent-free	0.3	15	84
4	0.01	Solvent-free	0.3	15	98
5	0.02	Solvent-free	0.3	15	98
6	0.01	H <sub>2</sub> O	0.3	15	50
7	0.01	PEG	0.3	15	49
8	0.01	EtOH	0.3	15	47
9	0.01	DMF	0.3	15	80
10	0.01	Solvent-free	0.2	15	90
11	0.01	Solvent-free	0.4	15	96

**Table 3.** Optimizing reaction conditions for oxidation of methyl phenyl sulfide in the presence of Fe<sub>3</sub>O<sub>4</sub>@SiO<sub>2</sub>@A-TT-Pd.

ethers of iodobenzene with phenol. According to the study, the yield of the product reached 58% in half of the reaction time. Subsequently, the experiment was replicated, and at the midpoint of the reaction, the catalyst was separated, allowing the filtrate to continue reacting. The yield at this stage amounted to 60%, thus confirming the absence of palladium leaching.

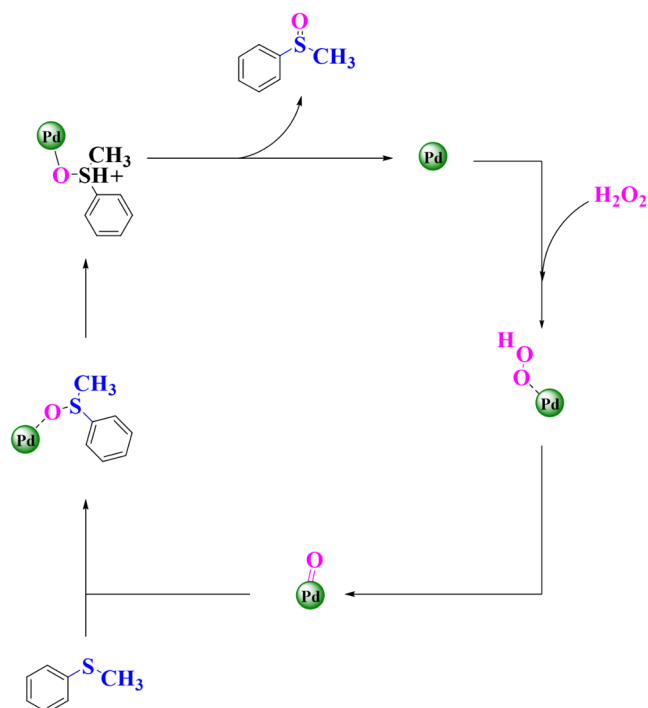
The ability to reuse catalysts is a crucial advantage, making them valuable for commercial use. We discovered that Fe<sub>3</sub>O<sub>4</sub>@SiO<sub>2</sub>@A-TT-Pd was rapidly recovered and displayed outstanding recyclability. To explore this, we examined the catalyst's recyclability in the oxidation of methyl phenyl sulfide. Following the reaction, the catalyst was isolated, rinsed with ethanol to eliminate any remaining product, and dried. Fresh substrates were then introduced to the remaining catalyst for the subsequent reaction. As depicted in Fig. 9, this catalyst can be reused for up to 5 cycles without experiencing significant loss of catalytic activity or Pd leaching.

#### Comparison of catalyst

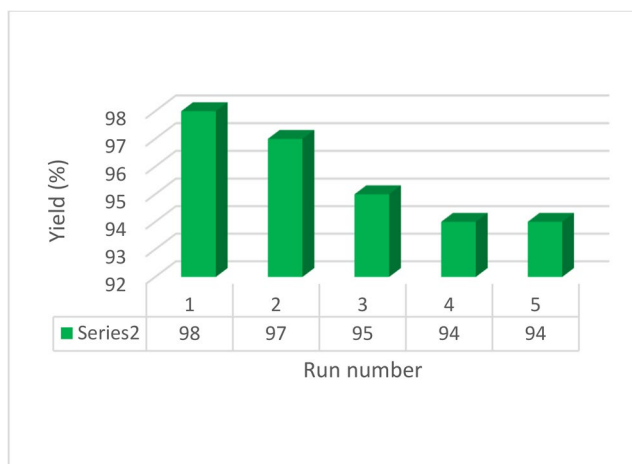
To explain the catalytic activity of Fe<sub>3</sub>O<sub>4</sub>@SiO<sub>2</sub>@A-TT-Pd, we analyzed the outcomes of methylphenyl sulfide oxidation using this catalyst and compared them with previously documented methods (Table 5). Notably, in contrast to other catalysts, the preparation of Fe<sub>3</sub>O<sub>4</sub>@SiO<sub>2</sub>@A-TT-Pd is straightforward using cost-effective and readily available materials, and it can be reused up to five times with no significant decline in activity. This catalyst results in a favorable reaction time and higher yield when compared to others. As a result, this novel catalyst demonstrates comparable or even superior characteristics in terms of cost, non-toxicity, stability, and ease of separation.

$\text{R-S-R} \xrightarrow[\text{Solvent-free, H}_2\text{O}_2, \text{ r.t.}]{\text{Fe}_3\text{O}_4@\text{SiO}_2@\text{A-TT-Pd}} \text{R-S(=O)-R}$						
Entry	Substrate	Product	Time(min)	Yield (%)	TON	TOF (h <sup>-1</sup> )
1			30	98	408	960
2			40	95	395.8	658
3			20	90	375	1250
4			30	92	383.3	766.6
5			20	87	362.5	1208
6			45	93	387.5	516
7			60	86	358.3	358.3
8			20	95	395.8	1319
9			35	95	395.8	682.4
10			20	90	375	1250

**Table 4.** Oxidation of sulfides into sulfoxides in the presence of Fe<sub>3</sub>O<sub>4</sub>@SiO<sub>2</sub>@A-TT-Pd.



**Scheme 5.** The suggested mechanism for the oxidation of sulfide.



**Fig. 9.** Recyclability of Fe<sub>3</sub>O<sub>4</sub>@SiO<sub>2</sub>@A-TT-Pd in the oxidation of sulfide.

Entry	Substrate	Catalyst	Time (min)	Yield (%)	Ref.
1	Ph-SCH <sub>3</sub>	Ni-dithizone@boehmite	80	96	<a href="#">29</a>
2	Ph-SCH <sub>3</sub>	Cu-SB-APT@MCM-41	45	91	<a href="#">30</a>
3	Ph-SCH <sub>3</sub>	Polymer-anchored Cu (II)	180	90	<a href="#">31</a>
4	Ph-SCH <sub>3</sub>	VO <sub>2</sub> F(dmpz) <sub>2</sub>	300	95	<a href="#">32</a>
5	Ph-SCH <sub>3</sub>	SiO <sub>2</sub> -W <sub>2</sub> -Im	150	91	<a href="#">33</a>
6	Ph-SCH <sub>3</sub>	Fe <sub>3</sub> O <sub>4</sub> @SiO <sub>2</sub> @A-TT-Pd	15	98	This work

**Table 5.** Comparing Fe<sub>3</sub>O<sub>4</sub>@SiO<sub>2</sub>@A-TT-Pd for oxidation of methyl phenyl sulfide with previously reported procedures.

## Conclusion

In summary, we have reported  $\text{Fe}_3\text{O}_4@\text{SiO}_2@\text{A-TT-Pd}$  as a green, efficient, and reusable catalyst for the oxidation of sulfides to sulfoxides and the synthesis of a wide range of diaryl ether derivatives. Both activity and selectivity in  $\text{Fe}_3\text{O}_4@\text{SiO}_2@\text{A-TT-Pd}$  are much higher than other previous catalysts. These protocols offer numerous benefits, including the utilization of readily available, cost-effective, environmentally friendly, and chemically stable materials, as well as straightforward operation and high to excellent yields. The simple procedure for preparation, use of non-toxic solvents, short reaction time, excellent tolerance of our method towards different functional groups, and the ability to recycle and reuse the catalyst using an external magnet up to five times with only a minor decrease in product yields are several advantages of this method. Furthermore, the  $\text{Fe}_3\text{O}_4@\text{SiO}_2@\text{A-TT-Pd}$  is more cost-effective and environmentally friendly due to its low Pd leaching.

## Data availability

All data generated or analyzed during this study are included in this published article and its supplementary information files.

Received: 3 July 2024; Accepted: 7 October 2024

Published online: 25 October 2024

## References

- Nikoorazm, M. et al. Synthesis of a new complex of lanthanum on MCM-41 as an efficient and reusable heterogeneous catalyst for the chemoselective synthesis of sulfoxides and tetrahydrobenzo[b]pyrans. *J. Porous Mater.* **31**, 511–526 (2024).
- Emad-Abbas, N., Naji, J., Moradi, P. & Kikhavani, T. 3-(Sulfamic acid)-propyltriethoxysilane on biochar nanoparticles as a practical, biocompatible, recyclable and chemoselective nanocatalyst in organic reactions. *RSC Adv.* **14**, 22147–22158 (2024).
- Rostami, A. et al. Silica sulfuric acid-coated  $\text{Fe}_3\text{O}_4$  nanoparticles as high reusable nanocatalyst for the oxidation of sulfides into sulfoxides, protection and deprotection of hydroxyl groups using HMDS and  $\text{Ac}_2\text{O}$ . *J. Saudi Chem. Soc.* **21**, 399–407 (2017).
- Jabbari, A., Nikoorazm, M. & Moradi, P. Two Schiff-base complexes of cadmium and manganese on modified MCM-41 as practical, recyclable and selective nanocatalysts for the synthesis of sulfoxides. *J. Porous Mater.* **30**, 1395–1402 (2023).
- Zhang, J. et al. Preparation of core/shell-structured  $\text{ZnFe}_2\text{O}_4@\text{ZnIn}_2\text{S}_4$  catalysts and its ultrafast microwave catalytic reduction performance for aqueous  $\text{Cr(VI)}$ . *Chem. Eng. J.* **451**, 138182 (2023).
- Yang, B. et al. The roles of  $\text{ZnFe}_2\text{O}_4$  and  $\alpha\text{-Fe}_2\text{O}_3$  in the biphasic catalyst for the oxidative dehydrogenation of n-butene. *J. Catal.* **381**, 70–77 (2020).
- Yao, L. et al. A rational design of  $\text{CdS}/\text{ZnFe}_2\text{O}_4/\text{Cu}_2\text{O}$  core-shell nanorod array photoanode with stair-like type-II band alignment for highly efficient bias-free visible-light-driven  $\text{H}_2$  generation. *Appl. Catal. B* **268**, 28, (2020).
- Wu, H., Hao, L., Chen, C. & Zhou, J. Superhydrophobic  $\text{Fe}_3\text{O}_4/\text{OA}$  magnetorheological fluid for removing oil slick from water surfaces effectively and quickly. *ACS Omega*. **5**, 27425–27432 (2020).
- Pinto, V. H. A. et al. Mn porphyrins immobilized on non-modified and chloropropyl-functionalized mesoporous silica SBA-15 as catalysts for cyclohexane oxidation. *Appl. Catal. A*. **526**, 9–20 (2016).
- Jammi, S. et al.  $\text{CuO}$  nanoparticles catalyzed C–N, C–O, and C–S cross-coupling reactions: scope and mechanism. *J. Org. Chem.* **74**, 1971–1976 (2009).
- Singh, P., Mishra, S., Sahoo, A. & Patra, S. A magnetically retrievable mixed-valent  $\text{Fe}_3\text{O}_4@\text{SiO}_2/\text{Pd}^0/\text{Pd}^{\text{II}}$  nanocomposite exhibiting facile tandem Suzuki coupling/transfer hydrogenation reaction. *Sci. Rep.* **11**, 9305 (2021).
- Ashraf, M. A., Liu, Z., Zhang, D. & Alimoradi, A. L-lysine-Pd complex supported on  $\text{Fe}_3\text{O}_4$  MNPs: a novel recoverable magnetic nanocatalyst for Suzuki C–C Cross-Coupling reaction. *Appl. Organomet. Chem.* **34**, e5668 (2020).
- Kanchana, U. S., Diana, E. J., Mathew, T. V. & Anilkumar, G. Palladium-catalyzed cross-coupling reactions of coumarin derivatives: an overview. *Appl. Organomet. Chem.* **34**, (2020).
- Lakshmidhevi, J., Naidu, B. R. & Venkateswarlu, K.  $\text{CuI}$  in biorenewable basic medium: three novel and low E-factor Suzuki–Miyaura cross-coupling reactions. *Mol. Catal.* **522**, 112237 (2022).
- Chen, J., Zhang, J., Zhang, Y., Xie, M. & Li, T. Nanoporous phenanthroline polymer locked Pd as highly efficient catalyst for Suzuki–Miyaura Coupling reaction at room temperature. *Appl. Organomet. Chem.* **34**, e5310, (2020).
- Lei, D. et al. Oxalate enhanced synergistic removal of chromium(VI) and arsenic(III) over  $\text{ZnFe}_2\text{O}_4/\text{g-C}_3\text{N}_4$ : Z-scheme charge transfer pathway and photo-Fenton like reaction. *Appl. Catal. B* **282**, 119578, (2021).
- Han, C. et al. Enhanced support effects in single-atom copper-incorporated carbon nitride for photocatalytic Suzuki cross-coupling reactions. *Appl. Catal. B*. **320**, 121954 (2023).
- Li, C. J. Reflection and perspective on green chemistry development for chemical synthesis - daoist insights. *Green Chem.* **18**, 1836–1838 (2016).
- Johansson Seechurn, C. C. C., Kitching, M. O., Colacot, T. J. & Snieckus, V. Palladium-catalyzed cross-coupling: a historical contextual perspective to the 2010 nobel prize. *Angewandte Chemie - Int. Ed.* **51**, 5062–5085 (2012).
- Jia, Y. et al. Recent advances in doping strategies to improve Electrocatalytic Hydrogen Evolution performance of Molybdenum Disulfide. *ACS Catal.* **14**, 4601–4637 (2024).
- Geissel, F., Lang, L., Husemann, B., Morgan, B. & Deponte, M. Deciphering the mechanism of glutaredoxin-catalyzed roGFP2 redox sensing reveals a ternary complex with glutathione for protein disulfide reduction. *Nat. Commun.* **15**, 1733 (2024).
- Karami, M. & Aghabarari, B. The Advancement of Molybdenum Disulfide Quantum dots nanoparticles as Nanocarrier for Drug Delivery systems: cutting-edge in dual therapeutic roles. *J. Mol. Struct.* **139149** <https://doi.org/10.1016/j.molstruc.2024.139149> (2024).
- Sekar, P. et al. Regiodivergent synthesis of 4- and 5-Sulphenyl oxazoles from Alkynyl Thioethers. *Chem. – Eur. J. n/a*, **40**, e202401465 (2024).
- Li, X. R., Zhang, R. J., Xiao, Y., Tong, Q. X. & Zhong, J. J. N-Sulphenyl phthalimide enabled Markovnikov hydrothiolation of unactivated alkenes via ligand promoted cobalt catalysis. *Org. Chem. Front.* **11**, 646–653 (2024).
- Wang, P. et al. Thiosuccinimide enabled S–N bond formation to access N-sulphenylated sulfonamide derivatives with synthetic diversity. *Org. Biomol. Chem.* **22**, 990–997 (2024).
- Balajirao Dapkekar, A., Naveen, J. & Satyanarayana, G. Electrochemical Annulation of Ortho-Alkynylbiphenyls to Fused Sulphenyl Phenanthrenes and Spiro Cyclohexenone Indenes. *Adv. Synth. Catal.* **366**, 18–23 (2024).
- Zhang, F., Shen, B., Jiang, W., Yuan, H. & Zhou, H. Hydrolysis extraction of diosgenin from Dioscorea Nipponica Makino by sulfonated magnetic solid composites. *J. Nanopart. Res.* **21**, 12 (2019).
- Dindarloo Inaloo, I., Majnooni, S., Eslahi, H. & Esmaeilpour, M. N-Arylation of (hetero)arylamines using aryl sulfamates and carbamates via C–O bond activation enabled by a reusable and durable nickel(0) catalyst. *New J. Chem.* **44**, 13266–13278 (2020).

29. Ghorbani-Choghamarani, A., Moradi, P. & Tahmasbi, B. Nickel(II) immobilized on dithizone–boehmite nanoparticles: as a highly efficient and recyclable nanocatalyst for the synthesis of polyhydroquinolines and sulfoxidation reaction. *J. Iran. Chem. Soc.* **16**, 511–521 (2019).
30. Nikoorazm, M., Rezaei, Z. & Tahmasbi, B. Two Schiff-base complexes of copper and zirconium oxide supported on mesoporous MCM-41 as an organic–inorganic hybrid catalysts in the chemo and homoselective oxidation of sulfides and synthesis of tetrazoles. *J. Porous Mater.* **27**, 671–689 (2020).
31. Islam, S. M. et al. Selective oxidation of sulfides and oxidative bromination of organic substrates catalyzed by Polymer anchored Cu(II) complex. *Tetrahedron Lett.* **53**, 127–131 (2012).
32. Hussain, S., Talukdar, D., Bharadwaj, S. K. & Chaudhuri, M. K. VO<sub>2</sub>F(dmpz)<sub>2</sub>: a new catalyst for selective oxidation of organic sulfides to sulfoxides with H<sub>2</sub>O<sub>2</sub>. *Tetrahedron Lett.* **53**, 6512–6515 (2012).
33. Thurow, S. et al. Base-free oxidation of thiols to disulfides using selenium ionic liquid. *Tetrahedron Lett.* **52**, 640–643 (2011).

## Acknowledgements

The authors extend their appreciation to King Saud University, Saudi Arabia, for funding this work through Researchers Supporting Project number (RSP2024R397), King Saud University, Riyadh, Saudi Arabia.

## Authors' contributions

Durgesh Singh. Kamini Singh. Pawan Sharma. Yashwantsinh Jadeja. Johar MGM. Priyanka Singh. Kiranjeet Kaur. M. Atif. Mohammed A. El-Meligy and Beneen Hussein Funding acquisition, Conceptualization, Resources, Supervision, Writing-review & editing.

## Declarations

### Competing interests

The authors declare no competing interests.

### Additional information

**Supplementary Information** The online version contains supplementary material available at <https://doi.org/10.1038/s41598-024-75681-x>.

**Correspondence** and requests for materials should be addressed to D.S.

**Reprints and permissions information** is available at [www.nature.com/reprints](http://www.nature.com/reprints).

**Publisher's note** Springer Nature remains neutral with regard to jurisdictional claims in published maps and institutional affiliations.

**Open Access** This article is licensed under a Creative Commons Attribution 4.0 International License, which permits use, sharing, adaptation, distribution and reproduction in any medium or format, as long as you give appropriate credit to the original author(s) and the source, provide a link to the Creative Commons licence, and indicate if changes were made. The images or other third party material in this article are included in the article's Creative Commons licence, unless indicated otherwise in a credit line to the material. If material is not included in the article's Creative Commons licence and your intended use is not permitted by statutory regulation or exceeds the permitted use, you will need to obtain permission directly from the copyright holder. To view a copy of this licence, visit <http://creativecommons.org/licenses/by/4.0/>.

© The Author(s) 2024